Organic Geochemistry 175 (2023) 104542

Contents lists available at ScienceDirect

Organic Geochemistry

journal homepage: www.elsevier.com/locate/orggeochem

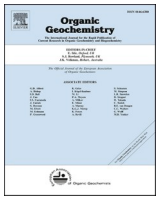

Mangrove sediment erosion in the Sunda Shelf during meltwater pulses: Insights from biomarker records

Jinyong Yu [a], Li Li [a,*], Xinkang Zhang [a], Juan He [a], Guodong Jia [a], Wolfgang Kuhnt [b]

[a] State Key Laboratory of Marine Geology, School of Ocean and Earth Science, Tongji University, Shanghai, China
[b] Institute of Geosciences, Christian-Albrechts-Universität, Kiel, Germany

ARTICLE INFO

Associate Editor–**Rienk Smittenberg**

Keywords:
Mangroves
Lipid biomarkers
Meltwater pulse events
Sea-level change
Sunda Shelf

ABSTRACT

Mangroves have received increasing attention in recent years for their high carbon storage capacity. The effects of sea-level change during the last glacial period on terrestrial deposition and coastal mangrove ecosystems were investigated using various organic lipid proxies in marine sediment cores from the Sunda Shelf in the southern South China Sea (SCS). The gradual reduction in the content of long-chain *n*-alkanes and *n*-alkanols, BIT index, and increasing $\delta^{13}C_{org}$ trend from the last glacial to the Holocene indicated that the depocenter moved landward from the studied location during the deglacial sea-level rise. Remarkable peaks in the mangrove proxy (Taraxerol/*n*-C_{28} alcohol ratio) occurred during meltwater pulse (MWP) events in the Sunda Shelf area, associated with the drowning and destruction of mangroves that could not withstand the rapid sea-level rise. The decomposition of carbon-rich mangrove deposits may have contributed to atmospheric CO_2 concentration during two strong MWP events in Sunda Shelf. Our results suggest the vulnerability of mangrove systems upon rapid sea level change with positive feedback for global warming.

1. Introduction

Global warming, caused by the increasing concentrations of atmospheric carbon dioxide, and global sea-level rise which threatens the lives of human populations in coastal zones, has become a significant problem in the 21st century (IPCC, 2021). Mangrove wetlands, one of the unique ecosystems in the intertidal zone in tropical and subtropical regions, play an essential role in conserving marine biodiversity, influencing biogeochemical processes, and regulating the global carbon budget (Brander et al., 2012; Wang and Gu, 2021). Although coastal mangroves account for only 0.5% of the world's coastal area, they contribute approximately 10–15% (23–32 Tg C yr^{-1}) to organic carbon burial in the coastal sediment, because of their higher area-normalized carbon burial rates than terrestrial forests (Donato et al., 2011; Alongi, 2014; Jennerjahn, 2021). Moreover, in contrast to decades or centuries of carbon storage capacity in tropical rainforests (Chambers et al., 2001), the longevity of mangrove carbon sinks is long, with carbon sequestered over the short term (decades) in biomass and longer time scales (millennia) in sediments (Duarte et al., 2005; McKee et al., 2007).

Global climate change (e.g., sea-level rise) can destroy mangrove ecosystems and affect their carbon sequestration rates (Sasmito et al., 2016). With global warming, the increased frequency of extreme weather events, such as hurricanes and storm surges, may also contribute to significant changes in coastal wetlands which can directly affect the growth and ecological functions of mangrove plants or even death (Cahoon et al., 2003; Lovelock et al., 2015). Without the protective layer provided by vegetation cover, the carbon-rich beds under mangroves may be eroded by wave action resulting in the loss of already buried carbon back to the atmosphere (Cahoon et al., 2003; Mcleod et al., 2011). Thus, knowledge of the fate of carbon sequestered in mangrove wetlands, especially under inundated or eroded conditions, and their impact on the carbon cycle is very important.

Pollen counts are one of the methods used in tracing the history of mangrove development (Scourse et al., 2005; Wooller et al., 2007; Borges da Silva et al., 2022). However, this method is limited since it is time consuming and has large sampling requirements for statistical analysis. Moreover, mangrove taxon is often over-represented in pollen diagrams of marine sediments due to their proximity to the ocean and high pollen production (Versteegh et al., 2004).

Lipid biomarkers, due to high preservation efficiency, have been increasingly used to characterize the sources of sedimentary organic matter and past environmental reconstruction in soils, lacustrine, and

* Corresponding author.
E-mail address: lilitju@tongji.edu.cn (L. Li).

https://doi.org/10.1016/j.orggeochem.2022.104542
Received 22 July 2022; Received in revised form 15 December 2022; Accepted 15 December 2022
Available online 20 December 2022

marine sediments (Castañeda and Schouten, 2011). Pentacyclic triterpenoids, frequently identified in higher plants and sediments, are generally regarded as mangrove-derived organic matter, i.e., taraxerol, β-amyrin, germanicol, and lupeol, which can even provide chemotaxonomic information (Killops and Frewin, 1994; Koch et al., 2003, 2011; Versteegh et al., 2004; Ranjan et al., 2015; Kumar et al., 2019a; Ratnayake et al., 2019). Relatively, taraxerol is more resistant to microbial degradation and it is the most abundant triterpenol in mangrove sediments, thus making it an ideal marker for mangroves, especially the *Rhizophora* genus (Johns et al., 1994; Versteegh et al., 2004; Koch et al., 2005, 2011; Kristensen et al., 2008; Ranjan et al., 2015; Gayantha et al., 2020). Therefore, taraxerol has been widely used in mangrove studies, e.g., in east Brazil (Koch et al., 2011; Kumar et al., 2019a; Carreira et al., 2021), south China (Chu et al., 2020), south India (Ranjan et al., 2015), and/or to trace mangrove ecosystem changes, e.g., Holocene history in southwest Sri Lanka (Ratnayake et al., 2017, 2019; Gayantha et al., 2020), last deglaciation variation in Congo fan (Kim et al., 2005; Scourse et al., 2005) and Amazon fan (Boot et al., 2006; Maslin et al., 2012), and mid-Pleistocene records in west Africa (Versteegh et al., 2004), etc.

The Sunda Shelf in Southeast Asia is a remarkably broad (800 km) and low gradient (ca. 0.03°) landmass ("Sundaland") with an area of ~ 1.8×10^6 km^2, which emerged and formed during the Last Glacial Maximum (LGM) low-stand (Hanebuth et al., 2011). Due to the flat shelf topography, the Sunda Shelf is sensitive to climate change-induced coastal dynamics, such as rapid sea-level rise (Hanebuth et al., 2000, 2009; Tjallingii et al., 2010), erosion (Steinke et al., 2008; Jiwarungrueangkul et al., 2019) and changes in sediment supply (Steinke et al., 2003, 2006). The melting of ice sheets during the last deglaciation led to a significant rise in sea level, flooding of coastal areas and changes in the oceanic coastlines.

Mangroves growing near the shorelines in Southeast Asia account for the most significant proportion of mangrove forests globally (Thomas et al., 2017). However, their response to sea-level fluctuations, especially the global meltwater pulse (MWP) events during the last deglacial period, are not clear, although limited palynological studies have indicated vegetation dynamics and relatively high mangrove percentages during the last glaciation (Sun et al., 2002; Wang et al., 2009; Luo et al., 2019; Kumar et al., 2019b; Yang et al., 2020). Therefore, this study presents record of long-chain alkanes, long-chain alkanols, and taraxerol in sediments from the southern South China Sea to trace changes in the terrestrial input and mangrove carbon reservoirs during the last deglaciation. The primary objectives are to evaluate: (1) the influence of local sea-level rise on terrestrial deposition, (2) the response of mangrove-derived sedimentary organic matter to MWP events, and (3) the deglacial evolution of mangrove ecosystem and implications on the carbon cycle and mangrove conservation.

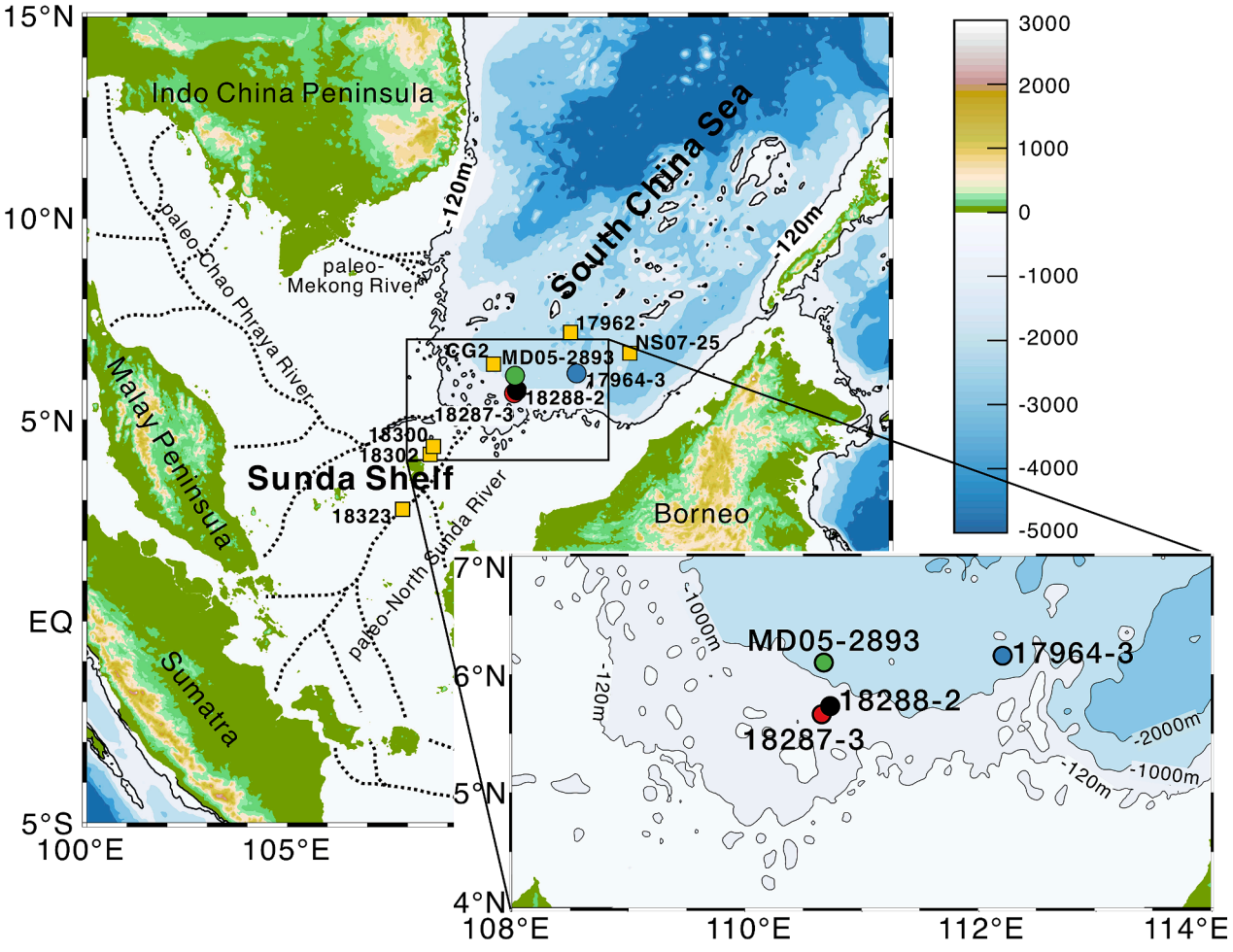

Fig. 1. Schematic map of the locations of the study sites in the southern South China Sea. The colored dots in the main map and inserted map indicate the main study sites. The orange squares show sites with records of mangrove pollen during the last glacial period (Sun et al., 2002; Wang et al., 2009; Kumar et al., 2019a; Luo et al., 2019; Yang et al., 2020). The location of paleo-coastline at low sea level during the last glacial period was around the 120 m isobath (solid black line) (Hanebuth et al., 2011). The glacial drainage systems (paleo-North Sunda River, paleo-Chao Phraya River and paleo-Mekong River) on the exposed Sunda Shelf during the glacial period are shown in black dashed lines (Voris, 2000).

2. Materials and methods

2.1. Sample collection and the age model

The sediment core 18288–2 (5°44.4′N, 110°44.3′E, water depth 788 m, core length 6.8 m) was retrieved from the upper continental slope outside the mouth of the paleo North Sunda River (Fig. 1) during the R/V *Sonne* cruise SO-115 in 1997 (Stattegger et al., 1997). The location of the sediment core allows monitoring of vegetation conditions on the shelf and changes in material supply of material from the shelf directly related to sea-level changes. Samples were collected in 10 cm intervals from the core repository kept at 4 °C, and stored at –20 °C before the organic lipids analyses.

The age model of the core 18288–2 was established based on planktonic foraminifera $\delta^{18}O$ records and Accelerator Mass Spectrometry (AMS) ^{14}C dating.

Thirty-four stable oxygen isotope values were obtained from well-preserved planktonic foraminifera *Globigerinoides ruber* (*G. ruber*) from the > 150 μm size fractions at 20 cm intervals (Fig. 3b), with a standard deviation of 0.07‰ for $\delta^{18}O$ values (Zhao et al., 2002, Cheng et al., 2005). The unexplainable abnormity of unusually low $\delta^{18}O$ reported in the bottom sample reported by Zhao et al. (2002), did not occur in our study. Seven AMS ^{14}C dating was performed on mixed planktonic foraminifera (*G. ruber* and *G. sacculifer*) due to insufficient mono-specific samples in this study. The radiocarbon dating was carried out at BETA Analytic laboratory (USA); the data were converted to calendar ages using "rbacon" package in Rstudio (Table 1), based on the "Marine20 calibration" dataset (Blaauw and Christen, 2011; Heaton et al., 2020) with a reservoir correction (ΔR) of − 125 ± 55 years, close to the value of − 143 ± 176 years in the Sunda Shelf (Wan et al., 2020). Because the past marine reservoir ages may vary significantly and are not well constrained, a constant reservoir age was chosen to calculate the calendar ages in the present study. The influence of age error caused by the uncertainties in the constant or varying ΔR is limited in the age-depth relationship differences (Huang et al., 2019). The final age model was established through interpolation and extrapolating between the age control points using "rbacon" package. The calculated age of core 18288–2 bottom sample was ~ 18.3 ka BP. The calculated sedimentation rate was significantly higher during the glacial period (average 70 cm/ka) than in the Holocene (average 20 cm/ka; Fig. 2), consistent with records reported for core 18287–3 (Kienast et al., 2001), 17964–3 (Wang et al., 1999), and MD01-2390 (Steinke et al., 2006) in the southern SCS.

The hemipelagic sediment core 17964–3 (6°9.5′N, 112°12.8′E, water depth 1556 m, core length 9.1 m) was retrieved during the R/V *Sonne* 95 cruises in 1994 (Fig. 1; Sarnthein et al., 1994). The age model and various organic and inorganic datasets in this core were extracted from published literatures (Wang et al., 1999; Pelejero et al., 1999; Pelejero, 2003; Steinke et al., 2003), except for the *n*-C_{28} alkanol and taraxerol concentrations which were determined in this study.

2.2. Analytical methods

2.2.1. Lipid extraction and analysis

Freeze-dried and homogenized sediment samples were ultrasonically extracted four times using dichloromethane (DCM):MeOH (1:1, v/v) for 15 min. Before extraction, known amounts of *n*-C_{19} alkanol, *n*-C_{36} alkane, and C_{46} glycerol trialkyl glycerol tetraether (GTGT) were added as internal standards. The supernatants were concentrated and saponified with 6% KOH/MeOH at 40 °C overnight to eliminate interferences from co-eluting wax esters (Villanueva et al., 1997). After saponification, neutral fractions were extracted with *n*-hexane and then separated into alkane, alcohol (including alkenones), and glycerol dialkyl glycerol tetraether (GDGT) subfractions using silica gel column by eluting with *n*-hexane, DCM, and MeOH, respectively. The alcohol fraction was further derivatized using N,O-*bis*(trimethylsilyl)-trifluoroacetamide (BSTFA) for 1 h at 70 °C before analysis.

Gas chromatographic (GC) analysis was conducted using a Thermo Trace GC Ultra equipped with a TG-5MS capillary column (60 m × 0.32 mm × 0.25 μm film thickness, Thermo Scientific) and a flame ionization detector (FID). Helium was used as a carrier gas with a flow velocity of 1.2 ml/min by splitless injection. Both the injector and detector were set at 300 °C. For the alkane fraction, the oven temperature was raised using the following temperature program: 80 °C for 1 min, 15 °C min^{-1} to 140 °C hold for 2 min, 10 min^{-1} to 220 °C hold for 2 min, 4 min^{-1} to 315 °C, and a final hold time of 30 min. For the alcohol fraction, the oven temperature was raised using the following temperature program: 80 °C for 1 min, 25 °C min^{-1} to 230 °C, 4 °C min^{-1} to 260 °C, hold for 2 min, 2 °C min^{-1} to 315 °C, and a final hold time of 45 min.

Selected samples were analyzed by GC–mass spectrometry (GC–MS) to confirm compound identification and the absence of co-elution problems. The GC–MS analysis was conducted using a Thermo Trace GC 1300 coupled to a Thermo TSQ 8000 Evo operating in electron impact (EI) mode with an emission electron energy of 70 eV, ion source temperature of 250 °C and mass range of *m/z* 50–600. The capillary column and temperature program used were the same as that of the GC analysis. The identification of *n*-C_{28} alkan-ol, taraxerol and $C_{37:2}$ alkenone were carried out by GC–MS using their retention times and diagnostic ions *m/z* 467, 204 and 530, respectively.

The *n*-alkanes and *n*-alkanols were confirmed by their retention times with the external standard *n*-alkanes and *n*-alkanols (Supelco, USA). Quantification was performed by comparing the relevant peak area with that of the internal standard. The average recoveries of alkane and alkanol were > 90% and > 85%, with uncertainty of about ± 2.5% and ± 3.5%, respectively. The conversion equation used for $U^{K'}_{37}$ and sea surface temperature (SST) was $U^{K'}_{37} = 0.031SST + 0.092$ (Pelejero and Grimalt, 1997).

The detailed method for GDGTs analysis has been reported elsewhere (Cao et al., 2020). Briefly, GDGTs were analyzed by high-performance liquid chromatography–atmospheric pressure chemical ionization-mass spectrometry (HPLC–APCI-MS, Agilent 1200 series 6460 QQQ) with two silica columns (150 mm × 2.1 mm × 1.9 μm, ThermoFinnigan)

Table 1
AMS-^{14}C ages and calibrated ages of core 18288–2.

Depth (cm)	Lab code	AMS-^{14}C age (yr BP ± 1σ)	Reservoir correction (ΔR) (yr ± 1σ)	Calibrated age (cal yr BP ± 1σ)
0–1	Beta-583246	220 ± 30	−125 ± 55	28 ± 28
55–56	Beta-583247	3410 ± 30	−125 ± 55	3260 ± 100
125–126	Beta-583248	6260 ± 30	−125 ± 55	6636 ± 105
175–176	Beta-583249	8540 ± 30	−125 ± 55	9127 ± 107
225–226	Beta-583250	10080 ± 40	−125 ± 55	11158 ± 98
375–376	Beta-583251	12740 ± 40	−125 ± 55	14498 ± 196
505–506	Beta-583252	13270 ± 40	−125 ± 55	15289 ± 137

All datings were performed on mixed species of *G. ruber* and *G. sacculifer*.

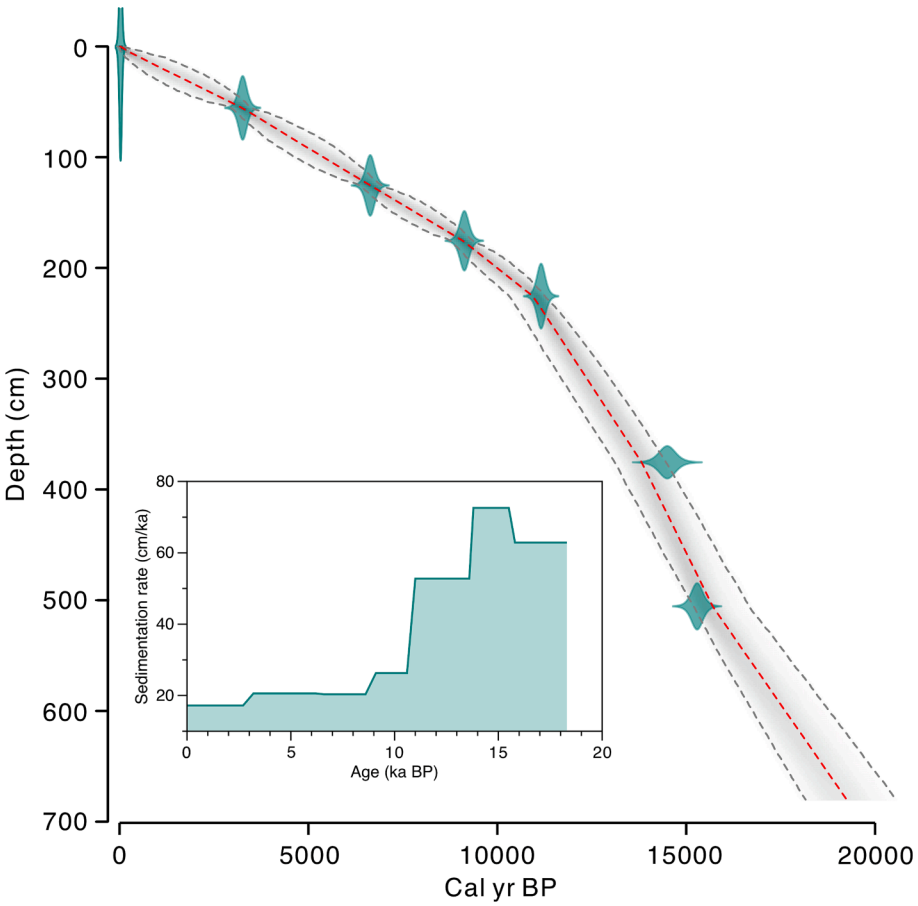

Fig. 2. Age-depth model and sedimentation rate of core 18288–2. The age-depth relationship was calculated using the "rbacon" package (Blaauw and Christen, 2011) overlying the distributions of the individual dates (green). Line curve shows the best model (red line: mean); the area between the dashed lines indicates chronological uncertainties (the model's 95% probability interval). The inset shows the sedimentation rate.

maintained at 40 °C. GDGTs were eluted at 0.2 ml/min with 84% hexane and 16% ethyl acetate for 5 min, followed by a linear gradient to 18% ethyl acetate in 60 min, then to 100% ethyl acetate in 21 min, subsequently back to 16% ethyl acetate in 4 min and held for 30 min. GDGTs were detected via selected single ion monitoring (SIM) of *m/z* 1292, 1050, 1048, 1046, 1036, 1034, 1032, 1022, 1020, 1018, 744 and quantified by comparing the peak area of each compound with that of the internal standard. The BIT (Branched vs Isoprenoid Tetraether) index, a soil input proxy, was defined as $\frac{[Ia]+[IIa]+[IIIa]+[IIa']+[IIIa']}{[Ia]+[IIa]+[IIIa]+[IIa']+[IIIa']+[Cren]}$ (Hopmans et al., 2004). The Roman numerals represent the different molecular structures of GDGTs as defined in De Jonge et al. (2014), and Cren represents crenarchaeol.

2.2.2. Bulk parameters

Samples for the analyses of total organic carbon (TOC) and stable organic carbon isotope ($\delta^{13}C_{org}$) composition were first decarbonated using a diluted HCl solution (1 M), then washed with distilled water and freeze-dried before testing. The contents of total carbon (TC) and TOC were analyzed using elemental analyzer (Vario EL cube), and $\delta^{13}C_{org}$ values were determined using an isotope ratio mass spectrometer (DELTA^{plus}XP) interfaced with the elemental analyzer (Carlo Erba Instruments Flash 1112). The analytical precisions of carbon content and $\delta^{13}C_{org}$ measurements were $< 0.1\%$ and $< 0.05‰$, respectively. The difference between TC and TOC concentrations was taken as the carbonate ($CaCO_3$) content, reported in % dry weight. Acetanilide from Indiana University with $\delta^{13}C$ value of –29.53 ± 0.01‰ was used as reference and analyzed before and after every 10 samples. The $\delta^{13}C_{org}$ values were expressed in standard delta notation relative to the Vienna Pee Dee Belemnite (VPDB) standards.

3. Results

In core 18288–2, the SST values determined from $U^{K'}_{37}$ varied from 24.8 °C to 27.8 °C with the lowest value in 14.7 ka BP and highest in the late Holocene. The most prominent feature is a 1.5 °C warming from the Heinrich Stadial event 1(HS1) to Bølling–Allerød period (B-A) (Fig. 3c). The $\delta^{13}C_{org}$ values varied between –25‰ and –22‰. The most negative $\delta^{13}C_{org}$ (–25‰) occurred during the period from 18.3 ka BP to 17 ka BP, increased by ~ 2‰ from 17 ka BP to 16 ka BP, and became stable between –23‰ and –22‰ after 16 ka BP (Fig. 3d). The *n*-C_{29} alkane and *n*-C_{28} alkanol exhibited similar trends, with high values of 570 ng/g and 717 ng/g occurring during the last glacial, while low contents of 50 ng/g and 105 ng/g were recorded in the Holocene, respectively. Overall, the concentrations of *n*-C_{28} alkanol were slightly higher and more variable than the *n*-C_{29} alkane concentrations (Fig. 3e,f). $CaCO_3$ contents ranged from < 0.1% to 20%, with low levels occurring before 16.5 ka BP, then gradually increased to ~ 20% in the middle to late Holocene, similar to records in the adjacent cores 18287-3 and 17964-3 (Fig. 3g) on the Sunda slope (Steinke et al., 2003).

The BIT index in core 18288–2 varied between 0.9 and 0.2, with high values during the glacial period (Fig. 3h). The BIT index exhibited a similar variation trend to the $\delta^{13}C_{org}$. A remarkable reduction in the BIT values (0.6) was recorded in the 17–16 ka BP time interval, and < 0.3 in the late Holocene which were comparable to the typical values in the deep-water areas of the South China Sea (Jia et al., 2012).

The content of taraxerol in core 18288–2 exhibited remarkable

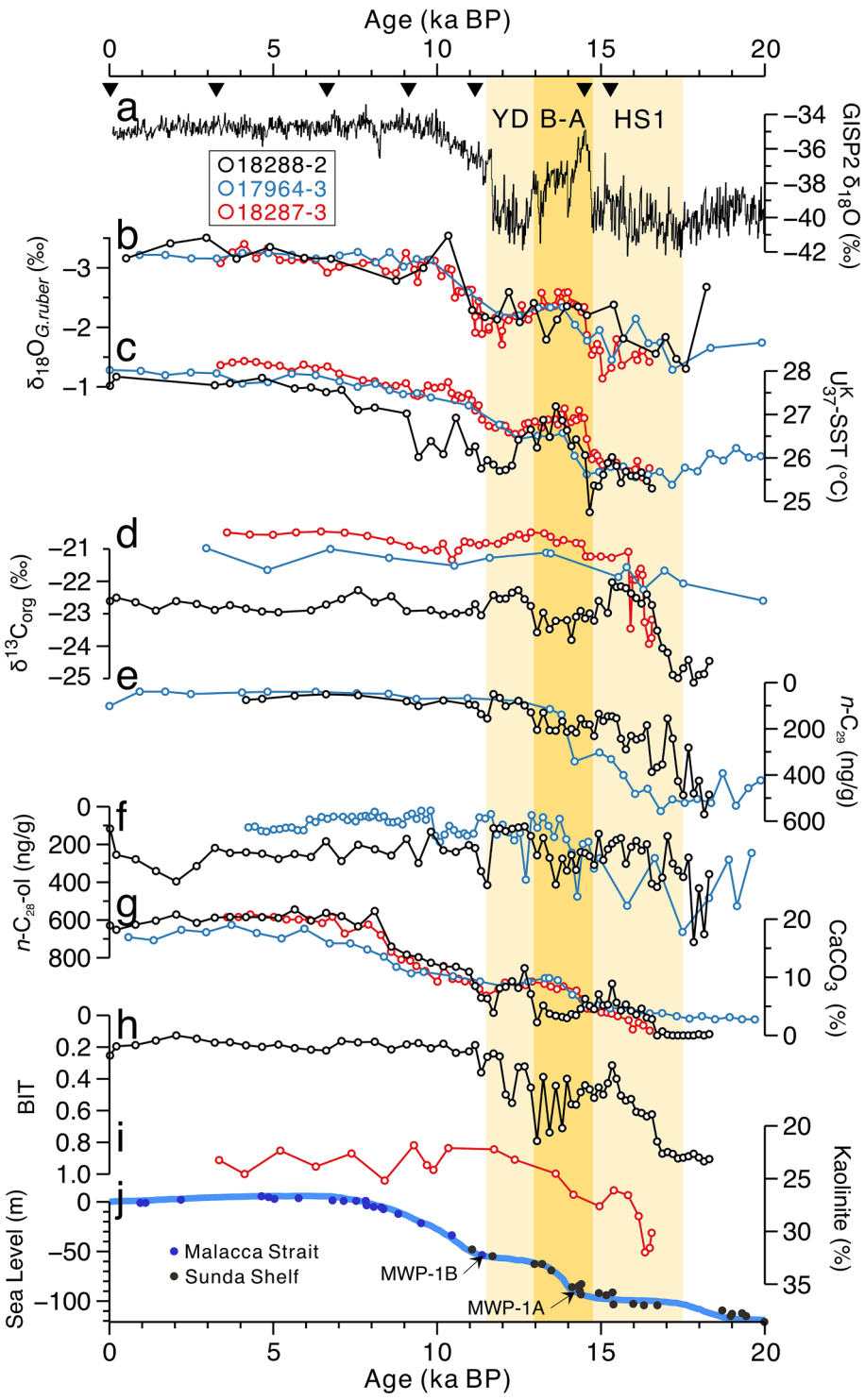

Fig. 3. Paleoclimate records and terrestrial input at the Sunda slope since the 20 ka BP. (a) $\delta^{18}O$ record of GISP2 ice core (Greenland) (Grootes and Stuiver, 1997), (b) $\delta^{18}O$ of *G. ruber* in core 18288–2 (black; Zhao et al., 2002), core 17964–3 (blue; Wang et al., 1999), core 18287–3 (red; Kienast et al., 2001), (c) $U^{K'}_{37}$ vs SST in core 18288–2 (black, this study); core 17964–3 (blue, Pelejero et al., 1999), core 18287–3 (red, Kienast et al., 2001), (d) $\delta^{13}C$ of organic carbon in core 18288–2 (black, this study); cores 17964–3 and 18287–3 (blue and red, respectively, Steinke et al., 2003), (e) *n*-C_{29} alkane concentration in core 18288–2 (black, this study); core 17964–3 (blue, Pelejero, 2003), (f) *n*-C_{28} alkanol concentration in cores 18288–2 and 17964–3 (black and blue, respectively, this study), (g) carbonate content in core 18288–2 (black, this study); cores 17964–3 and 18287–3 (blue and red, respectively, Steinke et al., 2003), (h) BIT index in core 18288–2 (black, this study), (i) kaolinite content in core 18287–3 (red; Steinke et al., 2008), and (j) estimated sea-level curve for the Sunda Shelf region (Geyh et al., 1979; Hanebuth et al., 2000). Triangles denote radiocarbon dates; shaded vertical bars show the major climate intervals: the Heinrich Stadial event 1 (HS1), the Bølling-Allerød period (B–A), and the Younger Dryas period (YD). MWP stands for melt water pulse.

variation. The minimum and maximum values were 60 ng/g and 1362 ng/g, respectively, with fluctuations around 150 ng/g except for several peaks occurring in 18.3–17.7 ka BP, 14.7–14.8 ka BP, 11.9–11.1 ka BP and 10.6–9.1 ka BP. The ratio of taraxerol to *n*-C_{28} alkanol (T/C_{28}-ol) varied between 2.9 and 0.3 in core 18288–2, depicting a trend similar to the taraxerol content with several sharp peaks superimposed on the relatively stable low values (Fig. 4b, c). The content of taraxerol and T/C_{28}-ol ratio in core 17964–3 with a longer time series were similar to those in core 18288–2 both in trend and contents (Fig. 4b,c).

4. Discussion

The $\delta^{18}O$ data in core 18288–2 was somewhat insufficient, and challenging to compare the results with other well-dated high-resolution foraminifera $\delta^{18}O$ records (e.g., core 18287–3; Kienast et al., 2001) in detail. Nevertheless, the synchronous abrupt warming during the Bølling Transition (14.7–14.2 ka BP) and gradual warming trend from YD to the early Holocene (12.0–10.5 ka BP) in the alkenone thermometry records in both core 18287-3 and core 18288–2 (Kienast et al., 2001) as shown in Fig. 3c indicated that the age model in this study performed

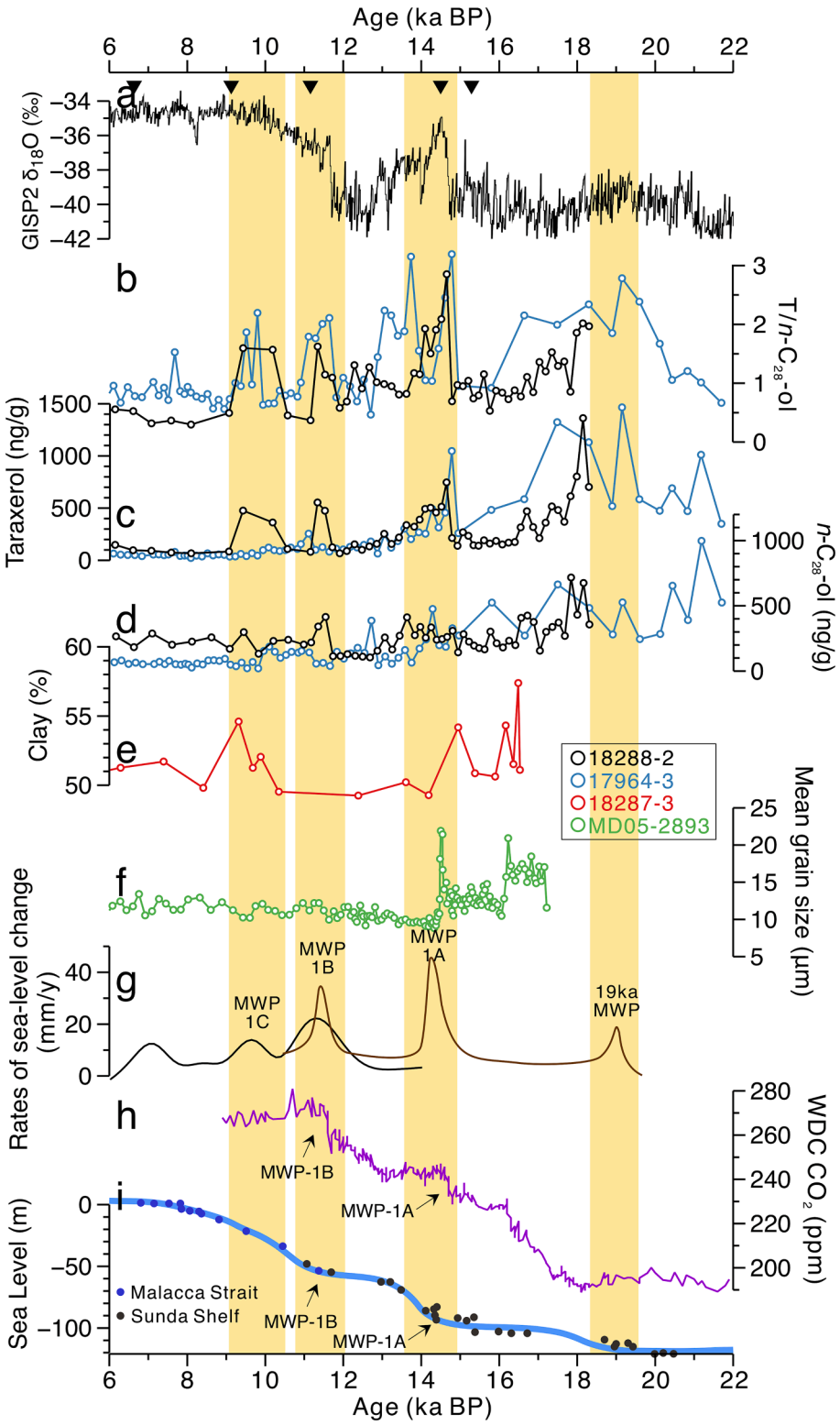

Fig. 4. Various index records since the 20 ka BP. (a) $\delta^{18}O$ record of GISP2 ice core (Greenland) (Grootes and Stuiver, 1997), (b) T/*n*-C_{28}-ol ratio in cores 18288–2 and 17964–3 (black and blue, respectively, this study, the same for curves c and d), (c) taraxerol concentration (ng/g) (d) *n*-C_{28} alkanol concentration (ng/g), (e) clay content (<2 μm) in core 18287–3 (Steinke et al., 2003), (f) mean grain size in core MD05-2893 (Jiwarungrueangkul et al., 2019), (g) rates of sea-level change (Red Sea in black line (Grant et al., 2012), Sunda Shelf in brown line (Hanebuth et al., 2000, 2009)), (h) atmosphere CO_2 concentration from WDC ice core (West Antarctica) (Marcott et al., 2014), (i) estimated sea-level curve for the Sunda Shelf region (Geyh et al., 1979; Hanebuth et al., 2000). Triangles denote radiocarbon dates; shaded vertical bars correspond to the 19 ka MWP, MWP-1A, MWP-1B, and MWP-1C periods.

satisfactorily and could be reliably used to discuss the findings of this study.

4.1. *Influence of local sea-level rise on terrestrial deposition*

In this study, the predominance of odd/even long-chain *n*-alkanes (C_{23}–C_{33}) and an even/odd predominance in the long-chain *n*-alkanols (C_{22}–C_{32}) in core 18288–2 revealed a typical higher-plant origin (Eglinton and Eglinton, 2008). The biomarkers *n*-C_{29} alkane (or *n*-C_{28} alkanol) had been used as a representation of terrestrial plants input due to their generally high concentrations and the significant positive correlations with the total long-chain *n*-alkanes (or *n*-alkanols) (Pelejero, 2003). Higher deposition of terrestrial plant leaf waxes during the last glaciation than in the Holocene (Fig. 3e,f), is consistent with findings reported in previous studies both in the northern and southern SCS (Hu et al., 2002; Pelejero, 2003; He et al., 2008; Huang and Tian, 2012; Li

et al., 2013). Due to the high resolution and the unique geographical location of core 18288–2, approaching the paleo-estuary of the paleo-North Sunda River during the glacial low-stand period (Voris, 2000), the present work provides more detailed information about the paleo-environmental changes in the study region, especially the timing and magnitude of the fluctuations of the terrestrial lipids.

Previous studies had shown that the sea-level started rising on the Sunda Shelf at ca. 19 ka BP with at least 10 m height (–114 m to –96 m) in about 500 years, which is also referred to as the 19 ka BP MWP event (Hanebuth et al., 2000, 2009, 2011). The gradual decreasing trend in the contents of *n*-C_{29} alkane and *n*-C_{28} alkanol content from 18.3 ka (possibly earlier), as shown in Fig. 3e,f, suggested that the paleo-estuary was gradually moving landward from the study station. The more significant fluctuation of plant leaf wax inputs in core 18288–2 (water depth 788 m) may have been related to the proximity to the river mouth, which may have experienced intensive hydrological activity and/or sediment re-working than in the core 17964-3 (water depth 1556 m), as supported by the large fluctuations of $\delta^{13}C_{org}$ in a close core 18287–3 (Fig. 3d; Steinke et al., 2003).

The $\delta^{13}C_{org}$ value close to –25‰ during the low-stand period in core 18288–2 (Fig. 3d) indicated the limited C_4 vegetation and dominant rainforests' contribution in the studied area with a typical $\delta^{13}C$ value of –17‰ and –27‰ for C_4 and C_3 plants, respectively (Deines, 1980; Hu et al., 2003), although a savanna-like ecosystem was previously proposed in the exposed Sundaland (Bird et al., 2005). The typical $\delta^{13}C_{org}$ values in mangrove environments (−26‰ to − 29‰; Xia et al. 2015; Khan et al., 2019) generally fall within the range found for rainforests. Therefore, the autochthonous marine organic matter and allochthonous terrestrial plants inputs, featured by carbon isotope values of –20‰ and –27‰, respectively (Deines, 1980), were considered as the main sources in the present sediment $\delta^{13}C$ of bulk organic carbon.

The increasing $\delta^{13}C_{org}$ values from about –25‰ in 17 ka BP to –22.4‰ in 16 ka BP in core 18288–2 indicated a significant reduction of terrestrial-derived organic matter during this period, consistent with the observation in a nearby site (Fig. 3d). This was also confirmed by the significant drop in BIT from 0.9 to 0.6 in core 18288–2 (Fig. 3h), and decrease in kaolinite content (i.e., the contribution of clays from the Malay Peninsula, Sumatra, and Thailand) from 33% to 26% in the nearby site 18287–3 (Fig. 3i; Steinke et al., 2008). These substantial variations and the slightly increasing concentrations of $CaCO_3$ during the same time interval (Fig. 3g), indicated an abrupt initiation of dynamical changes in the coastal environments in response to the start of the last deglacial climate, including the inundation of the lowermost part of the paleo-North Sunda River and the retreat of depocenter from the front of the paleo-estuary into the middle river course at this time interval (Hanebuth et al., 2003, 2009; Steinke et al., 2003).

However, the fluctuations in the contents of *n*-C_{29} alkane and *n*-C_{28} alkanol, $\delta^{13}C_{org}$ and BIT were relatively weak after 16 ka BP in the upper continental slope sites and did not respond to the apparent sea-level rise characterized by two distinct meltwater pulse events (MWP-1A and MWP-1B) (Hanebuth et al., 2011). This indicated less significant changes in the sedimentary environment for the terrestrial deposition, although progressive landward retreat of the coastline continued during this period. Meanwhile, the large fluctuation of *n*-C_{29} alkane and *n*-C_{28} alkanol concentrations compared to the relative stability of BIT index during the time interval of 16–18 ka BP, and the large variation in the BIT index compared to the lower variations in *n*-C_{29} alkane and *n*-C_{28} alkanol concentrations during the B-A period (Fig. 3e,f,h) might indicate different sensitivities or transport mechanisms of different organic indices in response to the environmental changes.

4.2. Increase in mangrove-derived sedimentary organic matter during the MWP events

Mangroves are unique coastal vegetation that covers ca. 60–75% of the shoreline in the tropics and subtropics and are sensitive to environmental changes. Owing to its refractory nature, the mangrove biomarker taraxerol is frequently found in sediments. The abundance of taraxerol relative to *n*-C_{29} alkane (T/*n*-C_{29}) or *n*-C_{28} alkanol (T/*n*-C_{28}-ol), which are common biomarkers for terrestrial higher plants, has been used to reconstruct past mangrove ecosystems (Versteegh et al., 2004; Kim et al., 2005; Scourse et al., 2005). In the present work, the T/*n*-C_{28}-ol ratio was chosen as the mangrove indicator due to the similar polarity of both compounds, which, to a large extent, reduces the bias caused by differential degradation during diagenesis or analytical experiments. The T/*n*-C_{28}-ol ratios displayed a similar trend as the taraxerol content (Fig. 4b,c), with higher ratios corresponding to a high influx of mangrove-derived sedimentary organic matter in the southern SCS. This indicated that mangroves growing along the river mouths and coast in the exposed Sundaland were the predominant source of terrestrial derived organic matter in the study site (Sun et al., 2002; Wang et al., 2009).

Interestingly, the pulses of higher inputs of mangrove-derived organic matter during 20–19 ka BP, 14.8–13.6 ka BP, 11.9–11.2 ka BP, and 10.6–9.1 ka BP were synchronous with the MWP events recorded in the Sundaland area with higher rates of sea-level rise (Hanebuth et al., 2000), especially during the MWP-1A and MWP-1B periods when the sea-level rising rates were ~ 38 mm/y and ~ 30 mm/y, respectively (Fig. 4b,g). Unlike the global signal of MWP-1A, there was no evidence for a global MWP-1B event at ~11.3 ka BP (Lambeck et al, 2014), but a rapid sea level rise was reported during this time interval in Barbados and Sunda Shelf regions (Hanebuth et al., 2000, 2009; Bard et al., 2010). Here, mangrove biomarker peaks during 11.3–11.5 ka BP corresponded extremely well with the MWP-1B event in both cores (Fig. 4b,c), similar to the MWP-1A event, indicating the close linkage between the rate of sea level rise and mangrove erosion in Sundaland. Such rates are much higher than the suggested threshold of ~ 6 mm/y for mangroves survival under a sea-level rising condition (Saintilan et al., 2020), implying intense decomposition of mangrove vegetation and sediments during the time intervals of rapid sea level rise.

A similar scenario had been reported in sediments off the west coast of Africa (Versteegh et al., 2004; Kim et al., 2005; Scourse et al., 2005). The relatively high mangrove-derived organic matter peak during the 19 ka BP MWP (a weak MWP event compared with MWP-1A and 1B) might be related to several factors, such as: (1) the low sea level and hence the proximity of the core to the paleo shoreline, where mangrove organic matter could be easily reached (Steinke et al., 2003); (2) the large extent of mangroves growing on the coastal area of the exposed shelf during the glacial period (Sun et al., 2002; Wang et al., 2009); and (3) the previous long period of sea-level stability that facilitated the maturation of mangrove communities (Hanebuth et al., 2011), thus, yielding more available mangrove materials. Notably, MWP-1C during the early Holocene (Fig. 3g), which is lacking in some records, was characterized by high T/*n*-C_{28}-ol ratios in the present work (Fig. 4b), possibly related to an abrupt transition from fluvial to marine deposition in Asia (Liu et al., 2004; Hori and Saito, 2007; Tjallingii et al., 2010).

After MWP-1C, especially after 6 ka BP, mangrove signals became weakened and/or below the detection limit in the studied sites due to their far distance from the coast and complete submergence of the Sundaland. Therefore, the increase in mangrove-derived sedimentary organic matter during the MWPs originated mainly from erosion of the original mangrove deposits.

The coastline is generally more susceptible to resuspension and in situ transport by erosion and disturbance without the protection from the overlying vegetation. Some depositional evidence in the Sunda Shelf area also reflected shoreline erosion during the periods of rapidly rising sea-level, consistent with the decrease in clay content (Fig. 4e) (Pelejero et al., 1999; Steinke et al., 2003), and increase in mean grain size (Fig. 4f) and sand proportions (Kienast et al., 2001; Jiwarungrueangkul et al., 2019). However, not all MWPs were recorded in previous studies due to low sample resolution or site location. Here, the presentation of the four MWP events by T/*n*-C_{28}-ol ratio in Sunda Shelf region indicated

the well-documented paleoceanographic changes by the organic lipids, which are very important in paleoceanography and paleoclimate studies.

4.3. Deglacial variation of the mangrove ecosystem and implications for the carbon cycle

Mangrove ecosystems generally serve as a significant long-term carbon sink with much higher area-normalized carbon burial rates and thus are regarded as an essential part of the "blue carbon" reservoirs, even though their wetlands could serve as a source of CH_4 and N_2O (Mcleod et al., 2011; Atwood et al., 2017; Hamilton and Friess, 2018). Mangroves can also capture suspended particles from upstream and the adjacent ocean by fluvial and tidal transportation, respectively (Alongi, 2014). However, if the mangrove vegetation is destroyed by natural forces and/or human activities, the subsequent erosion of mangrove deposits will likely act as a potential source of carbon.

In this study, the high inputs of mangrove-derived organic matter to the study sites suggested that mangroves could not keep pace with the accelerated sea-level rise (>15 mm/y) during MWPs. The drowned mangrove communities are confirmed by a large number of thick mangrove-rich peat beds, such as in the central and outer Sunda Shelf (Hanebuth et al., 2003, 2009), the Mekong River delta (Tamura et al., 2009; Li et al., 2012; Liu et al., 2017), the Chao Phraya River delta

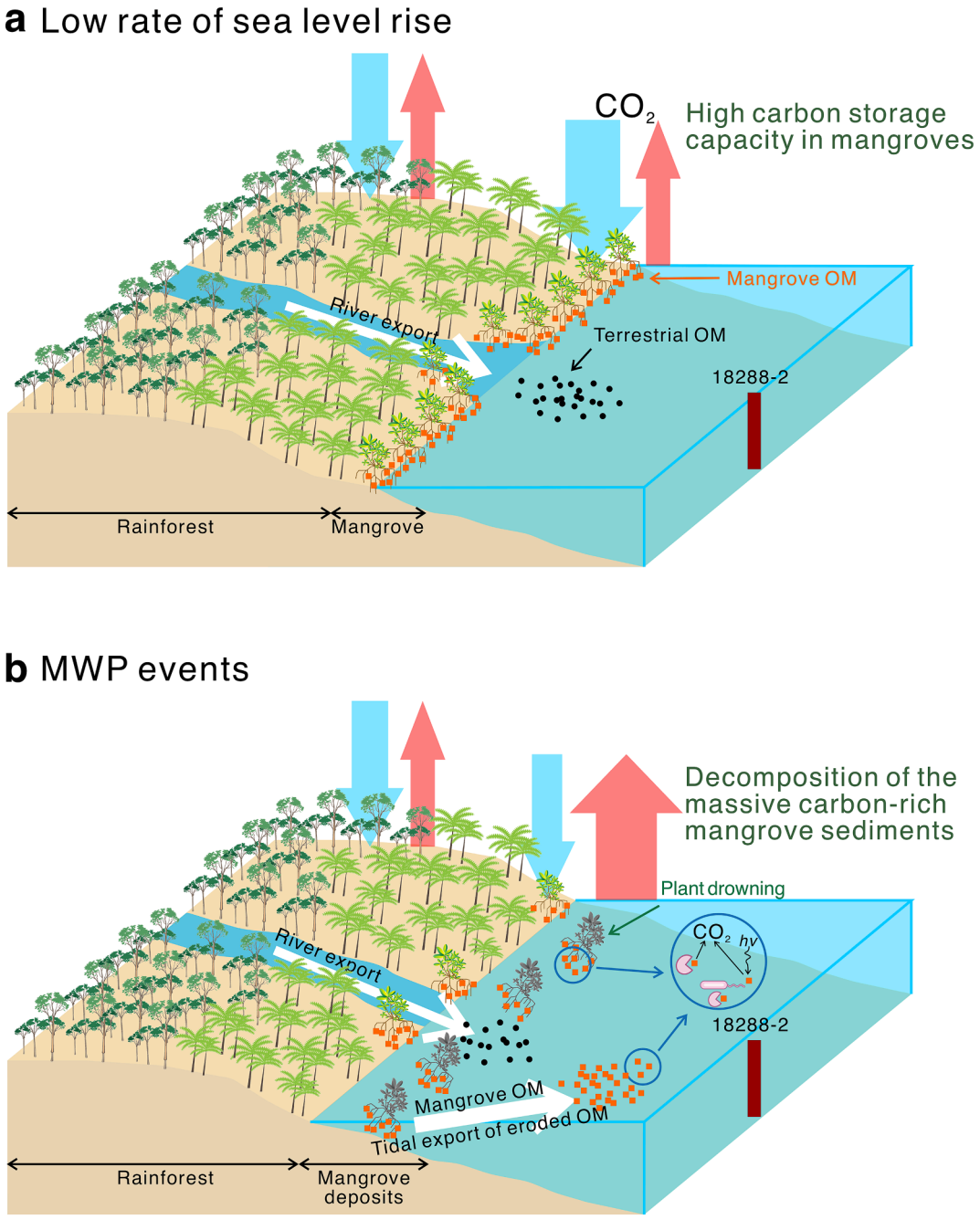

Fig. 5. Schematic diagram illustrating the response of terrestrial organic matter and mangrove organic matter to the rate of sea level change. (a) low rate of sea level rise, (b) rapid rate of sea level rise, such as the MWP events. The blue downward and red upward arrows indicate the carbon storage and release by the plants, with the left pairs for rainforests and right pairs for mangroves, respectively. The width of the arrows represents the carbon quantity, wide for great quantity and narrow for less quantity.

(Somboon, 1988), and the Gulf of Thailand (Somboon, 1988; Sinsakul, 1992). Significant amounts of taraxerol and other immature biogenic components have been previously reported in shelf sediments from the marginal Petrel Basin, the Timor Sea (northern Australia) since the LGM (Nicholas et al., 2014).

The root system of the vegetation plays a vital role in maintaining soil structure's stability; thus, the destruction of mangroves would lead to the collapse of the soil below (Cahoon et al., 2003). Moreover, without the protection from mangroves, most coastal areas would suffer severe erosion and hydraulic scouring, and rising sea-level would also exacerbate the erosive effects of storm surges and extreme astronomical tides on the coast (FitzGerald et al., 2008). Compared to the slow organic matter oxidation in anoxic mangrove soils (Chmura et al., 2003; Mckee et al., 2007), once submerged and eroded, the sequestered carbon in mangrove vegetation and deposits would be readily oxidized to CO_2, leading to carbon loss to the atmosphere (Fig. 5).

Intense coastal hydrodynamics would intensify this scenario during the deglacial sea-level rises, including slumping, tidal, and wave actions that would allow oxygen to penetrate deeper into the sedimentary carbon reservoirs (Abrams et al., 2018). The high T/*n*-C_{28}-ol ratios during the MWP-1A and 1B in our results corresponded with the two significant increases in atmospheric CO_2 concentration (Fig. 4h), suggesting that the erosion of mangrove sediment may act as a possible potential source of atmospheric carbon (Fig. 5). This premise is supported by a recent simulation study, which revealed that sizeable amounts of terrestrial carbon transferred to the ocean during MWP-1A triggered the local oceanic CO_2 outgassing and anomalies in oceanic parameters, such as sea surface alkalinity, dissolved inorganic carbon, and phosphate, particularly in Southeast Asia (Extier et al., 2022).

Although the high T/*n*-C_{28}-ol ratios corresponded well with increasing CO_2 concentration during MWP 1A and 1B events, the relatively stable pCO_2 during the 19 ka BP MWP and MWP 1C did not spontaneously change with high T/*n*-C_{28}-ol in Sunda Shelf during these periods. Because of the complex mechanism of pCO_2 variability, the increasing carbon release in the Sunda Shelf may possibly be counteracted by other processes globally. More paleo-mangrove records including the lipids, pollens as well as model simulations are required in future studies to estimate the variability of different carbon budgets in different time intervals for deeper understanding of the role of mangroves in the global carbon cycle.

Despite the inferred collapse and erosion of the mangrove ecosystem during the rapid sea-level rise of MWPs, our results suggest that mangroves did not disappear entirely and might have recovered to some extent as the T/*n*-C_{28}-ol ratio did not decline to zero (Fig. 4b). The general decreasing trend in the T/*n*-C_{28}-ol ratio from the last glacial to the Holocene could indicate the gradually increasing distance from the mangrove habitats to the study sites along with the sea-level rise. This implies that mangroves can recover rapidly once the sea-level rise slows down. Several recent studies have highlighted the horizontal and vertical adaptation of coastal wetlands, which would migrate to newly formed habitats due to sea-level changes (McKee et al., 2007; Schuerch et al., 2018). The flat topography of the Sunda Shelf may facilitate the landward extension of mangroves under a slow sea-level rise (i.e., $< \sim 6$ mm/y) and the preservation of high carbon-bearing sediments of the mangrove ecosystem (Woodroffe et al., 2016; Chen et al., 2020; Cheng et al., 2021). The increase in mangrove pollen content during the deglaciation period observed from the Sunda Shelf may also have supported the expansion of mangroves during that time (Wang et al., 2007, 2009).

4.4. Insights on the conservation of mangroves

According to the IPCC's latest projections (AR6) (IPCC, 2021), the rate of sea-level rise in the next century will reach 6 mm/y (or even $>$ 24 mm/y) based on the estimated GHG emission levels which would exceed the scenario at 19 ka BP MWP and MWP-1C during the last deglaciation period. Severe weather events, such as tropical cyclones and coastal floods caused by global warming are also increasing (Woodruff et al., 2013). Additionally, human activities, i.e., deforestation of mangroves, constructing of coastal dikes, highways and residential areas, are also severely reducing mangrove vegetative areas (Chmura et al., 2003; Mcleod et al., 2011; Alongi, 2014; Schuerch et al., 2018). All these show that mangroves are suffering from major threats both from natural disasters and increased human activities, especially in coastal areas. In the past years, approximately 1.04 million ha of mangrove forests vanished globally due to sea-level rise, deforestation, and land-use change (Lovelock et al., 2015; Bryan-Brown et al., 2020). Mangrove deposits, which are carbon-rich reservoirs formed on centennial to millennial scales (Duarte et al., 2005; Mckee et al., 2007), are difficult to recover on human time scales. Thus, the destruction of mangrove carbon reservoirs could have significant environmental and climate impacts. Based on the paleo record in Sunda Shelf, the erosion of mangrove deposits would contribute to increasing atmospheric CO_2 levels. At present, the conservation of mangrove ecosystem and protection from erosion, and damage by human activities are crucial for limiting the potential significant carbon loss from this valuable ecosystem.

5. Conclusions

Organic lipids were studied in sediment cores from the southern South China Sea, and the results revealed significant effects of sea-level change on terrestrial deposition. The distinctly decreasing trends in the concentrations of long-chain *n*-C_{29} alkane and *n*-C_{28} alkanol, BIT index, increasing $\delta^{13}C_{org}$ ratios and carbonate contents in core 18288–2 over the 17–16 ka BP time interval, indicated a dramatic change in the depositional environment associated with the inundation of the lowest part of the paleo-North Sunda River. The apparent abrupt increase in the content of taraxerol and T/*n*-C_{28}-ol ratio during 20–19 ka BP, 14.8–13.6 ka BP, 11.9–11.2 ka BP, and 10.6–9.1 ka BP were synchronous with the MWP events recorded in the Sunda Shelf area. This is the first report on simultaneous variations of mangrove vegetation and MWP events, indicating mangrove deposit erosions due to rapid sea-level rise, facilitated by MWP events. The obvious increasing concentrations of CO_2 during the two strong meltwater pulses (MWP-1A and MWP-1B) covariated with the peaks of mangrove signals, indicating contributions from mangroves sequestered carbon in the Sunda Shelf area. As one of the most carbon-rich ecosystems on Earth, this study highlights the need for mangrove ecosystem conservation and protection from natural erosion and anthropogenic damage. This will help improve the carbon storage capacities of mangrove ecosystems and reduce the potential carbon loss.

Data availability

Datasets related to this article can be found in the supplementary material.

Declaration of Competing Interest

The authors declare that they have no known competing financial interests or personal relationships that could have appeared to influence the work reported in this paper.

Data availability

The data that has been used is confidential.

Acknowledgements

We thank the crew and the scientific party of R/V *Sonne* cruise SO-115, which was funded by the German Ministry of Science and Education (BMBF). This study was supported by grants from the Ministry of Science and Technology of China (No. 2018YFE0202402), the Science and Technology Commission of Shanghai (No. 20590780200) and the

National Natural Science Foundation of China (Nos. 41876042; 41673042; 42030504; 41776049). Dr. John K. Volkman, Dr. Rienk Smittenberg, Dr. Nemiah Ladd and the anonymous reviewers are greatly appreciated for their constructive comments.

Appendix A. Supplementary data

Supplementary data to this article can be found online at https://doi.org/10.1016/j.orggeochem.2022.104542.

References

Abrams, J.F., Hohn, S., Rixen, T., Merico, A., 2018. Sundaland peat carbon dynamics and its contribution to the Holocene atmospheric CO_2 concentration. Global Biogeochemical Cycles 32, 704–719.

Alongi, D.M., 2014. Carbon cycling and storage in mangrove forests. Annual Review of Marine Science 6, 195–219.

Atwood, T.B., Connolly, R.M., Almahasheer, H., Carnell, P.E., Duarte, C.M., Ewers Lewis, C.J., Irigoien, X., Kelleway, J.J., Lavery, P.S., Macreadie, P.I., Serrano, O., Sanders, C.J., Santos, I., Steven, A.D.L., Lovelock, C.E., 2017. Global patterns in mangrove soil carbon stocks and losses. Nature Climate Change 7, 523–528.

Bard, E., Hamelin, B., Delanghe-Sabatier, D., 2010. Deglacial Meltwater Pulse 1B and Younger Dryas sea levels revisited with boreholes at Tahiti. Science 327, 1235–1237.

Bird, M.I., Taylor, D., Hunt, C., 2005. Palaeoenvironments of insular Southeast Asia during the Last Glacial Period: A savanna corridor in Sundaland? Quaternary Science Reviews 24, 2228–2242.

Blaauw, M., Christen, J., 2011. Flexible paleoclimate age-depth models using an autoregressive gamma process. Bayesian Analysis 6, 457–474.

Boot, C.S., Ettwein, V.J., Maslin, M.A., Weyhenmeyer, C.E., Pancost, R.D., 2006. A 35,000 year record of terrigenous and marine lipids in Amazon Fan sediments. Organic Geochemistry 37, 208–219.

Borges da Silva, F.A., França, M.C., Cohen, M.C.L., Pessenda, L.C.R., Mayle, F.E., Fontes, N.A., Lorente, F.L., Junior, A.Á.B., Piccolo, M.de C., Bendassolli, J.A., Macario, K., Culligan, N., 2022. Late Holocene mangrove dynamics of the Doce River delta, southeastern Brazil: Implications for the understanding of mangrove resilience to sea-level changes and channel dynamics. Palaeogeography, Palaeoclimatology, Palaeoecology 600, 111055.

Brander, L.M., Wagtendonk, A.J., Hussain, S.S., McVittie, A., Verburg, P.H., de Groot, R. S., van der Ploeg, S., 2012. Ecosystem service values for mangroves in Southeast Asia: A meta-analysis and value transfer application. Ecosystem Services 1, 62–69.

Bryan-Brown, D.N., Connolly, R.M., Richards, D.R., Adame, F., Friess, D.A., Brown, C.J., 2020. Global trends in mangrove forest fragmentation. Scientific Reports 10, 7117.

Cahoon, D.R., Hensel, P., Rybczyk, J., McKee, K.L., Proffitt, C.E., Perez, B.C., 2003. Mass tree mortality leads to mangrove peat collapse at Bay Islands, Honduras after Hurricane Mitch. Journal of Ecology 91, 1093–1105.

Cao, J.T., Duan, X.Y., Jin, X.B., Lian, E.G., Yin, P., Li, L., Jia, G.D., 2020. Sedimentary core brGDGTs in the East China Sea are mainly produced in situ as evidenced by their similar distributions with brGDGTs derived from intact polar lipids. Organic Geochemistry 149, 104095.

Carreira, R.S., de Albergaria-Barbosa, A.C.R., de Lara, P.M., Arguelho, M., Garcia, C.A.B., 2021. A lipid biomarker investigation of the sources and distribution of organic matter in river-influenced shelf sediments of NE Brazil. Organic Geochemistry 151, 104162.

Castañeda, I.S., Schouten, S., 2011. A review of molecular organic proxies for examining modern and ancient lacustrine environments. Quaternary Science Reviews 30, 2851–2891.

Chambers, J.Q., Higuchi, N., Tribuzy, E.S., Trumbore, S.E., 2001. Carbon sink for a century: Intact rainforests have a long-term storage capacity. Nature 410, 429.

Chen, Y., Huang, E., Schefuß, E., Mohtadi, M., Steinke, S., Liu, J., Martínez-Méndez, G., Tian, J., 2020. Wetland expansion on the continental shelf of the northern South China Sea during deglacial sea level rise. Quaternary Science Reviews 231, 106202.

Cheng, X.R., Huang, B.Q., Jian, Z.M., Zhao, Q.H., Tian, J., Li, J.R., 2005. Forami niferal isotopic evidence for monsoonal activity in the South China Sea: a present-LGM comparison. Marine Micropaleontology 54, 125–139.

Cheng, Z., Weng, C., Steinke, S., Mohtadi, M., 2021. Marine pollen records provide perspective on coastal wetlands through Quaternary sea-level changes. Ecological Indicators 133, 108405.

Chmura, G.L., Anisfeld, S.C., Cahoon, D.R., Lynch, J.C., 2003. Global carbon sequestration in tidal, saline wetland soils. Global Biogeochemical Cycles 17, 1111.

Chu, M., Sachs, J.P., Zhang, H., Ding, Y., Jin, G., Zhao, M., 2020. Spatiotemporal variations of organic matter sources in two mangrove-fringed estuaries in Hainan. China. Organic Geochemistry 147, 104066.

De Jonge, C., Hopmans, E.C., Zell, C.I., Kim, J.-H., Schouten, S., Sinninghe Damsté, J.S., 2014. Occurrence and abundance of 6-methyl branched glycerol dialkyl glycerol tetraethers in soils: Implications for palaeoclimate reconstruction. Geochimica et Cosmochimica Acta 141, 97–112.

Deines, P., 1980. The isotopic composition of reduced organic carbon. In: Fritz, P., Fontes, J.C. (Eds.), The Terrestrial Environment. Handbook of Environmental Isotope Geochemistry, Elsevier, Amsterdam, pp. 329–406.

Donato, D.C., Kauffman, J.B., Murdiyarso, D., Kurnianto, S., Stidham, M., Kanninen, M., 2011. Mangroves among the most carbon-rich forests in the tropics. Nature Geoscience 4, 293–297.

Duarte, C.M., Middelburg, J.J., Caraco, N., 2005. Major role of marine vegetation on the oceanic carbon cycle. Biogeosciences 2, 1–8.

Eglinton, T.I., Eglinton, G., 2008. Molecular proxies for paleoclimatology. Earth and Planetary Science Letters 275, 1–16.

Extier, T., Six, K.D., Liu, B., Paulsen, H., Ilyina, T., 2022. Local oceanic CO_2 outgassing triggered by terrestrial carbon fluxes during deglacial flooding. Climate of the Past 18, 273–292.

FitzGerald, D.M., Fenster, M.S., Argow, B.A., Buynevich, I.V., 2008. Coastal impacts due to sea-level rise. Annual Review of Earth and Planetary Sciences 36, 601–647.

Gayantha, K., Routh, J., Anupama, K., Lazar, J., Prasad, S., Chandrajith, R., Roberts, P., Gleixner, G., 2020. Reconstruction of the Late Holocene climate and environmental history from North Bolgoda Lake, Sri Lanka, using lipid biomarkers and pollen records. Journal of Quaternary Science 35, 514–525.

Geyh, M.A., Kudrass, H.R., Streif, H., 1979. Sea-level changes during the late Pleistocene and Holocene in the Strait of Malacca. Nature 278, 441–443.

Grant, K.M., Rohling, E.J., Bar-Matthews, M., Ayalon, A., Medina-Elizalde, M., Beonk Ramsey, C., Satow, C., Roberts, A.P., 2012. Rapid response of ice volume to polar temperature variations. Nature 491, 744–747.

Grootes, P.M., Stuiver, M., 1997. Oxygen 18/16 variability in Greenland snow and ice with 10^{-3}- to 10^{5}-year time resolution. Journal of Geophysical Research: Oceans 102, 26455–26470.

Hamilton, S.E., Friess, D.A., 2018. Global carbon stocks and potential emissions due to mangrove deforestation from 2000 to 2012. Nature Climate Change 8, 240–244.

Hanebuth, T., Stattegger, K., Grootes, P.M., 2000. Rapid flooding of the Sunda Shelf: A late-glacial sea-level record. Science 288, 1033–1035.

Hanebuth, T.J.J., Stattegger, K., Schimanski, A., Lüdmann, T., Wong, H.K., 2003. Late Pleistocene forced-regressive deposits on the Sunda Shelf (Southeast Asia). Marine Geology 199, 139–157.

Hanebuth, T.J.J., Stattegger, K., Bojanowski, A., 2009. Termination of the Last Glacial Maximum sea-level lowstand: The Sunda-Shelf data revisited. Global and Planetary Change 66, 76–84.

Hanebuth, T.J.J., Voris, H.K., Yokoyama, Y., Saito, Y., Okuno, J., 2011. Formation and fate of sedimentary depocentres on Southeast Asia's Sunda Shelf over the past sea-level cycle and biogeographic implications. Earth-Science Reviews 104, 92–110.

He, J., Wang, P., Ge, H., 2008. Sea surface temperature and terrestrial biomarker records of the last 260 ka of core MD05-2904 from the northern South China Sea. Chinese Science Bulletin 53, 2376–2384.

Heaton, T.J., Köhler, P., Butzin, M., Bard, E., Reimer, R., Austin, W., Ramsey, C., Grootes, P., Hughen, K., Kromer, B., Reimer, P., Adkins, J., Burke, A., Cook, M., Olsen, J., Skinner, L., 2020. Marine20–The marine radiocarbon age calibration curve (0–55,000 cal BP). Radiocarbon 62, 1–42.

Hopmans, E.C., Weijers, J.W.H., Schefuß, E., Herfort, L., Sinninghe Damsté, J.S., Schouten, S., 2004. A novel proxy for terrestrial organic matter in sediments based on branched and isoprenoid tetraether lipids. Earth and Planetary Science Letters 224, 107–116.

Hori, K., Saito, Y., 2007. An early Holocene sea-level jump and delta initiation. Geophysical Research Letters 34, 2–6.

Hu, J., Peng, P., Jia, G., Fang, D., Zhang, G., Fu, J., Wang, P., 2002. Biological markers and their carbon isotopes as an approach to the paleoenvironmental reconstruction of Nansha area, South China Sea, during the last 30 ka. Organic Geochemistry 33, 1197–1204.

Hu, J., Peng, P., Fang, D., Jia, G., Jian, Z., Wang, P., 2003. No aridity in Sunda Land during the Last Glaciation: Evidence from molecular-isotopic stratigraphy of long-chain *n*-alkanes. Palaeogeography, Palaeoclimatology, Palaeoecology 201, 269–281.

Huang, E., Tian, J., 2012. Sea-level rises at Heinrich stadials of early Marine Isotope Stage 3: Evidence of terrigenous *n*-alkane input in the southern South China Sea. Global and Planetary Change 94–95, 1–12.

Huang, J., Wan, S.M., Li, A.C., Li, T.G., 2019. Two-phase structure of tropical hydroclimate during Heinrich Stadial 1 and its global implications. Quaternary Science Reviews 222, 105900.

IPCC, 2021. Summary for policymakers. In: Masson-Delmotte, V., Zhai, P., Pirani, A., Connors, S.L., Péan, C., Berger, S., Caud, N., Chen, Y., Goldfarb, L., Gomis, M.I., Huang, M., Leitzell, K., Lonnoy, E., Matthews, J.B.R., Maycock, T.K., Waterfield, T., Yelekçi, O., Yu, R., Zhou, B. (Eds.), Climate Change 2021: The Physical Science Basis. Contribution of Working Group I to the Sixth Assessment Report of the Intergovernmental Panel on Climate Change. Cambridge University Press, Cambridge, UK New York, USA, pp. 3–32.

Jennerjahn, T.C., 2021. Relevance and magnitude of "Blue Carbon" storage in mangrove sediments: carbon accumulation rates vs. stocks, sources vs. sinks. Estuarine. Coastal and Shelf Science 248, 107156.

Jia, G., Zhang, J., Chen, J., Peng, P., Zhang, C.L., 2012. Archaeal tetraether lipids record subsurface water temperature in the South China Sea. Organic Geochemistry 50, 68–77.

Jiwarungrueangkul, T., Liu, Z., Zhao, Y., 2019. Terrigenous sediment input responding to sea level change and East Asian monsoon evolution since the last deglaciation in the southern South China Sea. Global and Planetary Change 174, 127–137.

Johns, R.B., Brady, B.A., Butler, M.S., Dembitsky, V.M., Smith, J.D., 1994. Organic geochemical and geochemical studies of Inner Great Barrier Reef sediments—IV. Identification of terrigenous and marine sourced inputs. Organic Geochemistry 21, 1027–1035.

Khan, N.S., Vane, C.H., Engelhart, S.E., Kendrick, C., Horton, B.P., 2019. The application of $\delta^{13}C$, TOC and C/N geochemistry of mangrove sediments to reconstruct Holocene paleoenvironments and relative sea levels. Puerto Rico. Marine Geology 415, 105963.

Kienast, M., Steinke, S., Stattegger, K., Calvert, S.E., 2001. Synchronous tropical South China Sea SST change and Greenland warming during deglaciation. Science 291, 2132–2134.
Killops, S.D., Frewin, N.L., 1994. Triterpenoid diagenesis and cuticular preservation. Organic Geochemistry 21, 1193–1209.
Kim, J.H., Dupont, L., Behling, H., Versteegh, G.J.M., 2005. Impacts of rapid sea-level rise on mangrove deposit erosion: Application of taraxerol and *Rhizophora* records. Journal of Quaternary Science 20, 221–225.
Koch, B.P., Rullkötter, J., Lara, R.J., 2003. Evaluation of triterpenols and sterols as organic matter biomarkers in a mangrove ecosystem in northern Brazil. Wetlands Ecology and Management 11, 257–263.
Koch, B.P., Harder, J., Lara, R.J., Kattner, G., 2005. The effect of selective microbial degradation on the composition of mangrove derived pentacyclic triterpenols in surface sediments. Organic Geochemistry 36, 273–285.
Koch, B.P., Souza Filho, P.W.M., Behling, H., Cohen, M.C.L., Kattner, G., Rullkötter, J., Scholz-Böttcher, B., Lara, R.J., 2011. Triterpenols in mangrove sediments as a proxy for organic matter derived from the red mangrove (*Rhizophora mangle*). Organic Geochemistry 42, 62–73.
Kristensen, E., Bouillon, S., Dittmar, T., Marchand, C., 2008. Organic carbon dynamics in mangrove ecosystems: A review. Aquatic Botany 89, 201–219.
Kumar, M., Boski, T., Lima-Filho, F.P., Bezerra, F.H.R., González -Vila, F.J., Alam Bhuiyan, M.K., González-Pérez, J.A., 2019a. Biomarkers as indicators of sedimentary organic matter sources and early diagenetic transformation of pentacyclic triterpenoids in a tropical mangrove ecosystem. Estuarine, Coastal and Shelf Science 229, 106403.
Kumar, S., Luo, C., Xiang, R., Liu, J., Chen, C., Fang, X., 2019b. High-resolution palynological record for vegetation and environment change during MIS 2 in the southern South China Sea. Marine Micropaleontology 151, 101769.
Lambeck, K.H., Rouby, A., Purcell, A., Sun, Y., Sambridge, M., 2014. Sea level and global ice volumes from the Last Glacial Maximum to the Holocene. Proceedings of the National Academy of Sciences 111, 15296–15303.
Li, L., Li, Q., Tian, J., Wang, H., Wang, P., 2013. Low latitude hydro-climatic changes during the Plio-Pleistocene: Evidence from high resolution alkane records in the southern South China Sea. Quaternary Science Reviews 78, 209–224.
Li, Z., Saito, Y., Mao, L., Tamura, T., Li, Z., Song, B., Zhang, Y., Lu, A., Sieng, S., Li, J., 2012. Mid-Holocene mangrove succession and its response to sea-level change in the upper Mekong River delta, Cambodia. Quaternary Research 78, 386–399.
Liu, P., DeMaster, D., Nguyen, T., Saito, Y., Nguyen, V.L., Ta, T.K.O., Li, X., 2017. Stratigraphic formation of the Mekong River Delta and its recent shoreline changes. Oceanography 30, 72–83.
Liu, J.P., Milliman, J.D., Gao, S., Cheng, P., 2004. Holocene development of the Yellow River's subaqueous delta, North Yellow Sea. Marine Geology 209, 45–67.
Lovelock, C.E., Cahoon, D.R., Friess, D.A., Guntenspergen, G.R., Krauss, K.W., Reef, R., Rogers, K., Saunders, M.L., Sidik, F., Swales, A., Saintilan, N., Thuyen, L.X., Triet, T., 2015. The vulnerability of Indo-Pacific mangrove forests to sea-level rise. Nature 526, 559–563.
Luo, C., Haberle, S., Zheng, Z., Xiang, R., Chen, C., Lin, G., Sazal, K., 2019. Environmental changes in the north-east Sunda region over the last 40 000 years. Journal of Quaternary Science 34, 245–257.
Marcott, S.A., Bauska, T.K., Buizert, C., Steig, E.J., Rosen, J.L., Cuffey, K.M., Fudge, T.J., Severinghaus, J.P., Ahn, J., Kalk, M.L., McConnell, J.R., Sowers, T., Taylor, K.C., White, J.W.C., Brook, E.J., 2014. Centennial-scale changes in the global carbon cycle during the last deglaciation. Nature 514, 616–619.
Maslin, M.A., Ettwein, V.J., Boot, C.S., Bendle, J., Pancost, R.D., 2012. Amazon Fan biomarker evidence against the Pleistocene rainforest refuge hypothesis? Journal of Quaternary Science 27, 451–460.
McKee, K.L., Cahoon, D.R., Feller, I.C., 2007. Caribbean mangroves adjust to rising sea level through biotic controls on change in soil elevation. Global Ecology and Biogeography 16, 545–556.
Mcleod, E., Chmura, G.L., Bouillon, S., Salm, R., Björk, M., Duarte, C.M., Lovelock, C.E., Schlesinger, W.H., Silliman, B.R., 2011. A blueprint for blue carbon: toward an improved understanding of the role of vegetated coastal habitats in sequestering CO_2. Frontiers in Ecology and the Environment 9, 552–560.
Nicholas, W.A., Nichol, S.L., Howard, F.J.F., Picard, K., Dulfer, H., Radke, L.C., Carroll, A.G., Tran, M., Siwabessy, P.J.W., 2014. Pockmark development in the Petrel Sub-basin, Timor Sea, Northern Australia: Seabed habitat mapping in support of CO_2 storage assessments. Continental Shelf Research 83, 129–142.
Pelejero, C., 2003. Terrigenous *n*-alkane input in the South China Sea: High-resolution records and surface sediments. Chemical Geology 200, 89–103.
Pelejero, C., Grimalt, J.O., 1997. The correlation between the $U^{k'}_{37}$ index and sea surface temperatures in the warm boundary: The South China Sea. Geochimica et Cosmochimica Acta 61, 4789–4797.
Pelejero, C., Kienast, M., Wang, L., Grimalt, J.O., 1999. The flooding of Sundaland during the last deglaciation: Imprints in hemipelagic sediments from the southern South China Sea. Earth and Planetary Science Letters 171, 661–671.
Ranjan, R.K., Routh, J., Klump, J.V., Ramanathan, A.L., 2015. Sediment biomarker profiles trace organic matter input in the Pichavaram mangrove complex, southeastern India. Marine Chemistry 171, 44–57.
Ratnayake, A.S., Sampei, Y., Ratnayake, N.P., Roser, B.P., 2017. Middle to late Holocene environmental changes in the depositional system of the tropical brackish Bolgoda Lake, coastal southwest Sri Lanka. Palaeogeography, Palaeoclimatology, Palaeoecology 465, 122–137.
Ratnayake, A.S., Sampei, Y., Ratnayake, N.P., 2019. Characteristics of sedimentary organic matter and vascular plants in tropical brackish Bolgoda Lake, Sri Lanka: Implications for paleoecology and chemotaxonomy. Regional Studies in Marine Science 30, 100726.
Saintilan, N., Khan, N.S., Ashe, E., Kelleway, J.J., Rogers, K., Woodroffe, C.D., Horton, B. P., 2020. Thresholds of mangrove survival under rapid sea level rise. Science 368, 1118–1121.
Sarnthein, M., Pflaumann, U., Wang, P.X., Wong, H.K., 1994. Preliminary report of the Sonne-95 cruise "Monitor Monsoon" to the South China Sea. Berichte-Reports, Geologisch-Paläontologisches Institut und Museum, Christian-Albrechts-Universitaet Kiel 68.
Sasmito, S.D., Murdiyarso, D., Friess, D.A., Kurnianto, S., 2016. Can mangroves keep pace with contemporary sea level rise? A global data review. Wetlands Ecology and Management 24, 263–278.
Schuerch, M., Spencer, T., Temmerman, S., Kirwan, M.L., Wolff, C., Lincke, D., McOwen, C.J., Pickering, M.D., Reef, R., Vafeidis, A.T., Hinkel, J., Nicholls, R.J., Brown, S., 2018. Future response of global coastal wetlands to sea-level rise. Nature 561, 231–234.
Scourse, J., Marret, F., Versteegh, G.J.M., Jansen, J.H.F., Schefuß, E., van der Plicht, J., 2005. High-resolution last deglaciation record from the Congo fan reveals significance of mangrove pollen and biomarkers as indicators of shelf transgression. Quaternary Research 64, 57–69.
Sinsakul, S., 1992. Evidence of quarternary sea level changes in the coastal areas of Thailand: a review. Journal of Southeast Asian Earth Sciences 7, 23–37.
Somboon, J.R.P., 1988. Paleontological study of the recent marine sediments in the lower central plain, Thailand. Journal of Southeast Asian Earth Sciences 2, 201–210.
Stattegger, K., Kuhnt, W., Wong, H.K., and Scientific Party, 1997. Cruise Report SONNE 115 "SUNDAFLUT". Sequence stratigraphy, late Pleistocene–Holocene sea level fluctuations and high resolution record of the post-Pleistocene transgression on the Sunda Shelf. Berichte-Reports, Geologisch-Paläontologisches Institut und Museum, Christian-Albrechts-Universitaet Kiel 86.
Steinke, S., Kienast, M., Hanebuth, T., 2003. On the significance of sea-level variations and shelf paleo-morphology in governing sedimentation in the southern South China Sea during the last deglaciation. Marine Geology 201, 179–206.
Steinke, S., Chiu, H.Y., Yu, P.S., Shen, C.C., Erlenkeuser, H., Löwemark, L., Chen, M.T., 2006. On the influence of sea level and monsoon climate on the southern South China Sea freshwater budget over the last 22,000 years. Quaternary Science Reviews 25, 1475–1488.
Steinke, S., Hanebuth, T.J.J., Vogt, C., Stattegger, K., 2008. Sea level induced variations in clay mineral composition in the southwestern South China Sea over the past 17,000 yr. Marine Geology 250, 199–210.
Sun, X.J., Li, X., Luo, Y.L., 2002. Vegetation and climate on the Sunda shelf of the South China Sea during the last glaciation – pollen results from station 17962. Acta Botanica Sinica 44, 746–752.
Tamura, T., Saito, Y., Sieng, S., Ben, B., Kong, M., Sim, I., Choup, S., Akiba, F., 2009. Initiation of the Mekong River delta at 8 ka: evidence from the sedimentary succession in the Cambodian lowland. Quaternary Science Reviews 28, 327–344.
Thomas, N., Lucas, R., Bunting, P., Hardy, A., Rosenqvist, A., Simard, M., 2017. Distribution and drivers of global mangrove forest change, 1996–2010. PLoS One1 12, e0179302.
Tjallingii, R., Stattegger, K., Wetzel, A., Van Phach, P., 2010. Infilling and flooding of the Mekong River incised valley during deglacial sea-level rise. Quaternary Science Reviews 29, 1432–1444.
Versteegh, G.J.M., Schefuß, E., Dupont, L., Marret, F., Sinninghe Damsté, J.S., Jansen, J. H.F., 2004. Taraxerol and *Rhizophora* pollen as proxies for tracking past mangrove ecosystems. Geochimica et Cosmochimica Acta 68, 411–422.
Villanueva, J., Pelejero, C., Grimalt, J.O., 1997. Clean-up procedures for the unbiased estimation of C_{37} alkenone sea surface temperatures and terrigenous *n*-alkane inputs in paleoceanography. Journal of Chromatography A 757, 145–151.
Voris, H.K., 2000. Maps of Pleistocene sea levels in Southeast Asia: shorelines, river systems and time durations. Journal of Biogeography 27, 1153–1167.
Wan, J.X.W., Meltzner, A.J., Switzer, A.D., Lin, K., Wang, X., Bradley, S.L., Natawidjaja, D.H., Suwargadi, B.W., Horton, B.P., 2020. Relative sea-level stability and the radiocarbon marine reservoir correction at Natuna Island, Indonesia, since 6400 yr BP. Marine Geology 430, 106342.
Wang, Y.S., Gu, J.D., 2021. Ecological responses, adaptation and mechanisms of mangrove wetland ecosystem to global climate change and anthropogenic activities. International Biodeterioration and Biodegradation 162, 105248.
Wang, L., Sarnthein, M., Erlenkeuser, H., Grimalt, J., Grootes, P., Heilig, S., Ivanova, E., Kienast, M., Pelejero, C., Pflaumann, U., 1999. East Asian monsoon climate during the Late Pleistocene: high-resolution sediment records from the South China Sea. Marine Geology 156, 245–284.
Wang, X.M., Sun, X.J., Wang, P.X., Stattegger, K., 2007. A high-resolution history of vegetation and climate history on Sunda Shelf since the last glaciation. Science in China, Series D: Earth Sciences 50, 75–80.
Wang, X.M., Sun, X.J., Wang, P.X., Stattegger, K., 2009. Vegetation on the Sunda Shelf, South China Sea, during the Last Glacial Maximum. Palaeogeography, Palaeoclimatology, Palaeoecology 278, 88–97.
Woodroffe, C.D., Rogers, K., McKee, K.L., Lovelock, C.E., Mendelssohn, I.A., Saintilan, N., 2016. Mangrove sedimentation and response to relative sea-level rise. Annual Review of Marine Science 8, 243–266.

Wooller, M.J., Morgan, R., Fowell, S., Behling, H., Fogel, M., 2007. A multiproxy peat record of Holocene mangrove palaeoecology from Twin Cays, Belize. Holocene 17, 1129–1139.

Xia, P., Meng, X.W., Li, Z., Feng, A.P., Yin, P., Zhang, Y.Q., 2015. Mangrove development and its response to environmental change in Yingluo Bay (SW China) during the last 150 years: Stable carbon isotopes and mangrove pollen. Organic Geochemistry 85, 32–41.

Yang, Z., Li, T., Lei, Y., Chang, F., Nan, Q., 2020. Vegetation evolution-based hydrological climate history since LGM in southern South China Sea. Marine Micropaleontology 156, 101837.

Zhao, Q., Kuhnt, W., Stattegger, K., Cheng, X., 2002. Microfossils and paleoenvironments of the Sunda Slope of the South Cina Sea since the late Pleistocene. Marine Geology & Quaternary Geology 22, 63–68 in Chinese with English abstract.